

# SCIENTIFIC REPORTS



OPEN

## Electronic Structure and Band Gap Engineering of Two-Dimensional Octagon-Nitrogene

Wanxing Lin<sup>1</sup>, Jiesen Li<sup>2</sup>, Weiliang Wang<sup>1</sup>, Shi-Dong Liang<sup>1</sup> & Dao-Xin Yao<sup>1</sup>

A new phase of nitrogen with octagon structure has been predicted in our previous study, which we referred to as octagon-nitrogene (ON). In this work, we make further investigations of its stability and electronic structures. The phonon dispersion has no imaginary phonon modes, which indicates that ON is dynamically stable. Using *ab initio* molecular dynamic simulations, this structure is found to be stable up to room temperature and possibly higher, and ripples that are similar to that of graphene are formed on the ON sheet. Based on the density functional theory calculation, we find that single layer ON is a two-dimension wide gap semiconductor with an indirect band gap of 4.7 eV. This gap can be decreased by stacking due to the interlayer interactions. Biaxial tensile strain and perpendicular electric field can greatly influence the band structure of ON, in which the gap decreases and eventually closes as the biaxial tensile strain or the perpendicular electric field increases. In other words, both biaxial tensile strain and a perpendicular electric field can drive the insulator-to-metal transition, and thus can be used to engineer the band gap of ON. From our results, we see that ON has potential applications in many fields, including electronics, semiconductors, optics and spintronics.

Since the discovery of graphene, two-dimensional (2D) materials have attracted the attention of both theorists and experimentalists<sup>1</sup>. In the past several years, structures of new 2D materials have been proposed by theoretical prediction and confirmed by experiments<sup>2,3</sup>.

The research of 2D materials of group V is one of the foci in recent years<sup>4-7</sup>. The black phosphorus monolayer material has been investigated by first principle calculation, and prepared by mechanical exfoliation<sup>8,9</sup>. Using black phosphorus as a precursor, blue phosphorene, one of the three additional newly predicted phases of 2D structures of phosphorus, has been prepared by molecular beam epitaxial growth on Au(111)<sup>10</sup>. A stable 2D periodic atomic sheet consisting of carbon octagons, coined as octagraphene was proposed<sup>11</sup>, while the on-surface synthesis and electronic properties of graphene-like nanoribbons with periodically embedded four- and eight-membered rings was reported in reference<sup>12</sup>.

All of the monolayer of group V materials are insulators, and some of them have non-trivial topological properties. In contrast with graphene, the band structures of pnictogen monolayer can be controlled due to their intrinsic band gap. There are two techniques to control the band gap of monolayer pnictogen, either by the application of tensile strain or a perpendicular electric field<sup>13,14</sup>. Moreover, the band gap of the system decreases as the number of layers increases due to inter-layer couplings.

We have predicted two different structures of monolayer that consist of nitrogen atoms: honeycomb nitrogene and octagon-nitrogene (ON)<sup>15-17</sup>, and have investigated the existence and gap engineering of nitrogene<sup>16</sup>. It is interesting to notice that one zigzag ON nano-ribbon presents two linear bands, which might indicate the existence of a Dirac point<sup>17</sup>. In this paper, we further investigate the stability and band structure of ON. The stability of ON is further verified by phonon dispersion and first-principle molecular dynamics. In addition, we make more in-depth investigation of the electronic structures. More accurate band structures from hybrid functionals are obtained, and compared with our previous results calculated using pure functionals. Moreover, the band structure under biaxial tensile strain and in the presence of a perpendicular electric field is studied in detail, and we find that the electronic structure of ON can be controlled by adjusting both the strain and the field strength. These findings show that ON may be a promising material in some electronic devices<sup>18-22</sup>.

<sup>1</sup>State Key Laboratory of Optoelectronic Materials and Technologies, School of Physics, Sun Yat-Sen University, Guangzhou, P. R. China. <sup>2</sup>School of Environment and Chemical Engineering, Foshan University, Foshan, P. R. China. Correspondence and requests for materials should be addressed to D.-X.Y. (email: [yaodaoy@mail.sysu.edu.cn](mailto:yaodaoy@mail.sysu.edu.cn))

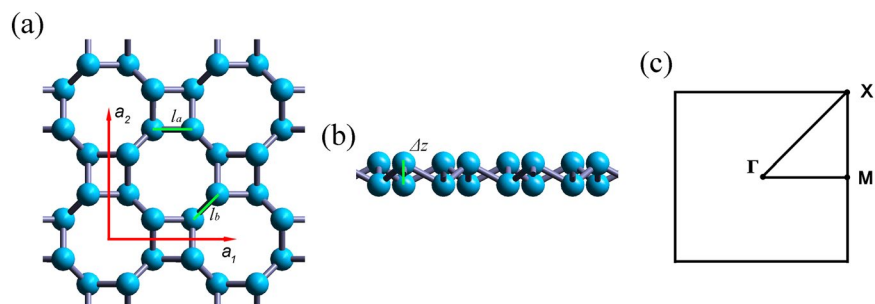


**Figure 1.** (a) Top view and (b) side view of ON. The red arrows  $a_1$ ,  $a_2$  show two basis vectors of the unit cell. (c) The first Brillouin zone and the high symmetry points.

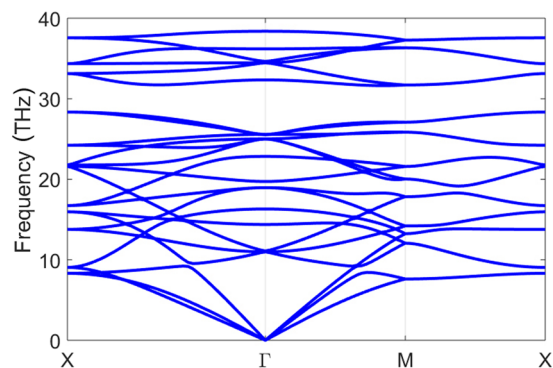


**Figure 2.** Phonon dispersion of ON monolayer.

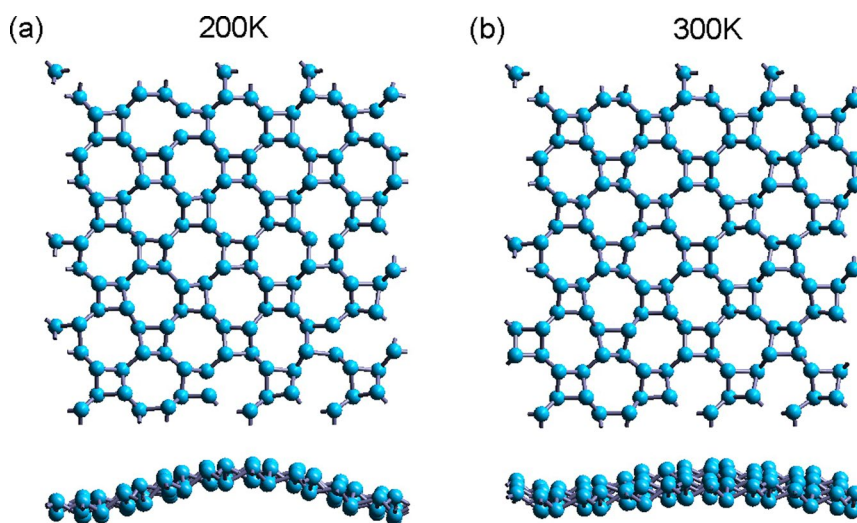


**Figure 3.** MD simulations of ON. The top and side views of the snapshots of the ON lattice structure in the MD simulations at 200 K (a), 300 K (b), respectively.

## Results

**Structure and Stability.** Figure 1 shows the geometric structure of ON. Each cell contains eight nitrogen atoms that are not coplanar. Hence, ON has buckling structure similar to nitrogene. Here,  $a$  is the lattice constant,  $l_a$  is the length of a bond in the square,  $l_b$  is the length of the bond connecting two squares, as shown in Fig. 1(a), the  $\Delta z$  is the buckling distance, as shown in Fig. 1(b)<sup>17</sup>.

The stable geometric structure of ON has been obtained by performing structure optimization in our previous work<sup>17</sup>. While in this paper, in order to investigate the stability of the ON, the phonon dispersion has been calculated, and the first principle MD simulations have been performed with over 2 picoseconds at 200 K and 300 K. From the phonon dispersion in Fig. 2, ON is found to be stable because no vibration modes with imaginary

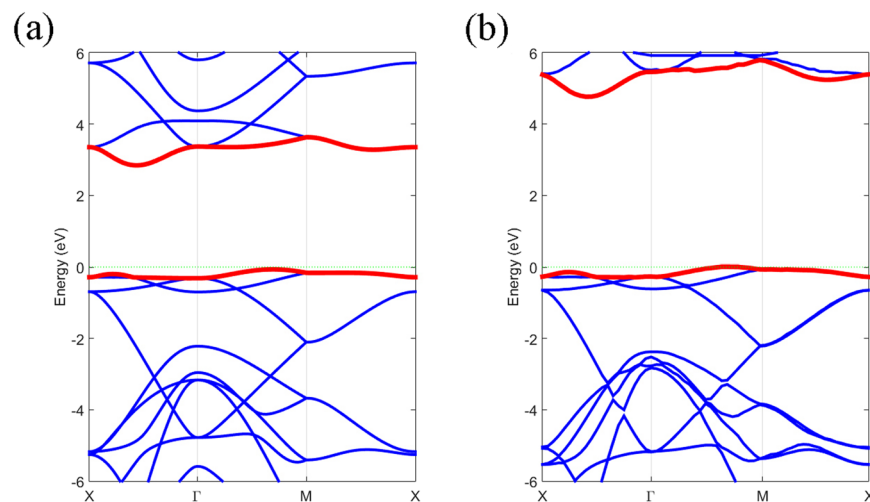


**Figure 4.** (a) The band structure calculated by PBE (a) and HSE (b) along high-symmetry points in the Brillouin zone. The energy is scaled with respect to the Fermi energy  $E_F$ . The red lines denote CBM and VBM, respectively.

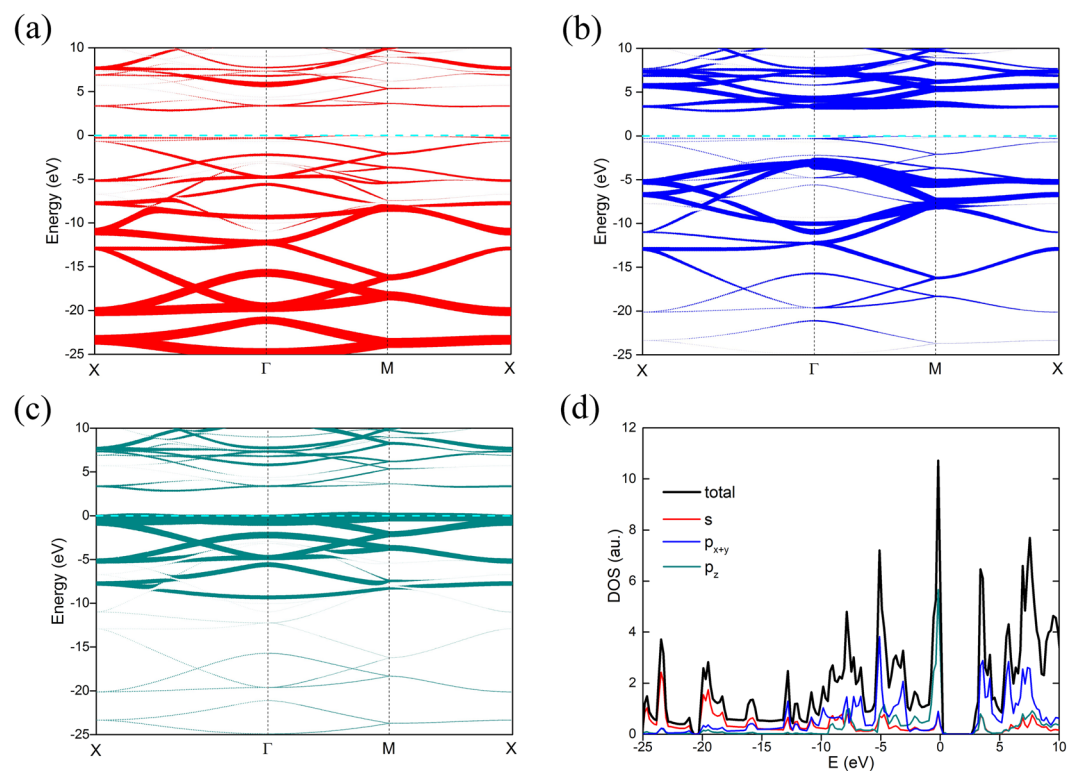


**Figure 5.** Projected electronic structure of ON. (a–c) Show the bands of s,  $p_{x+y}$  and  $p_z$  states, respectively, and the symbol size indicates the contribution weight. (d) The projected density of states of ON. Red, blue and dark cyan symbols denote the projections of the s,  $p_{x+y}$  and  $p_z$  states, respectively.

frequency are presented, the lowest phonon band near  $\Gamma$  point is highly firm. During the evolution of MD simulations, the sheet develops ripples along one of the axes, as shown in the snapshots in Fig. 3. The 2D ON lattice is dynamically stable at 200 K and 300 K without breaking the bonds, which indicates the structure is stable at room temperature.

**Electronic Structures of Single Layer and Multilayer.** The bands of free ON calculated by PBE without SOC are shown in Fig. 4(a) and the indirect band gap is 2.9 eV, which is the widest gap found in the octagon monolayer of group V elements<sup>17,23</sup>. Since pure functional tends to underestimate the band gap, we also calculated the

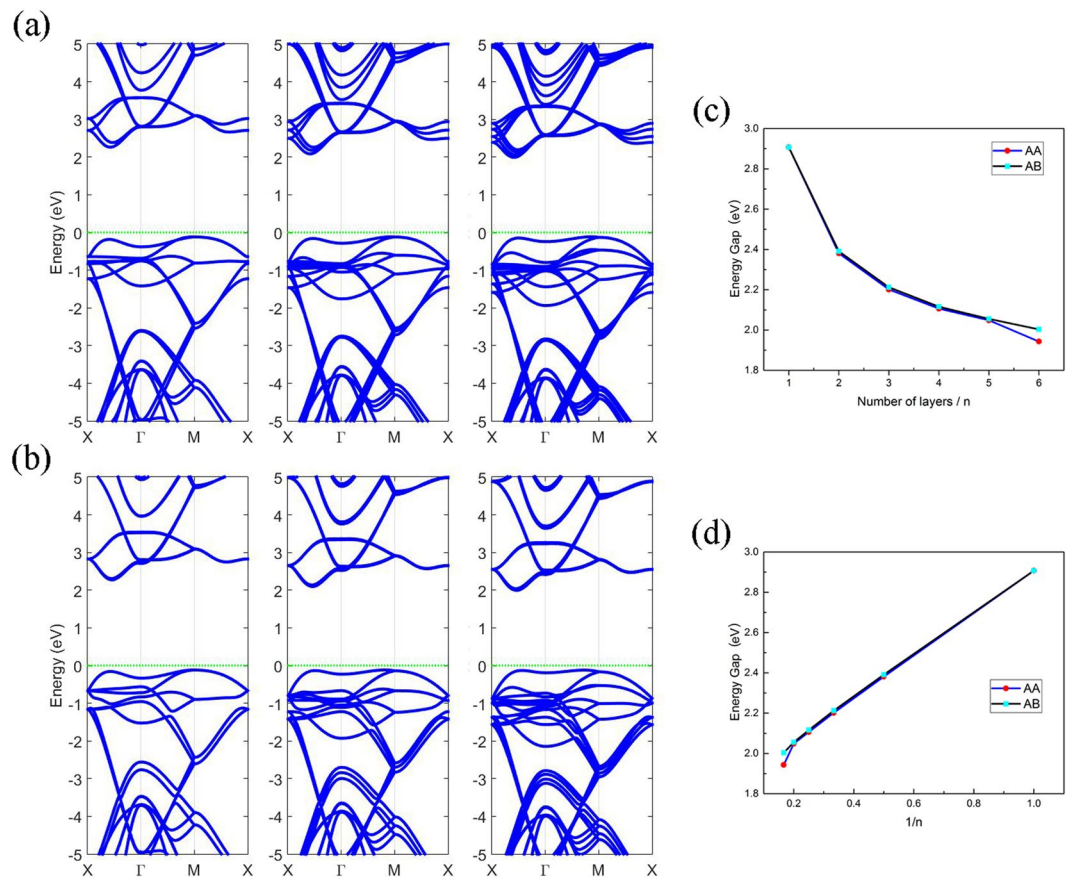


**Figure 6.** (a,b) Band structures of two, three, and four layers of ON for (a) AA stacking, and (b) AB stacking, respectively. (c–d) Show the dependence of band gap on the number of layers.

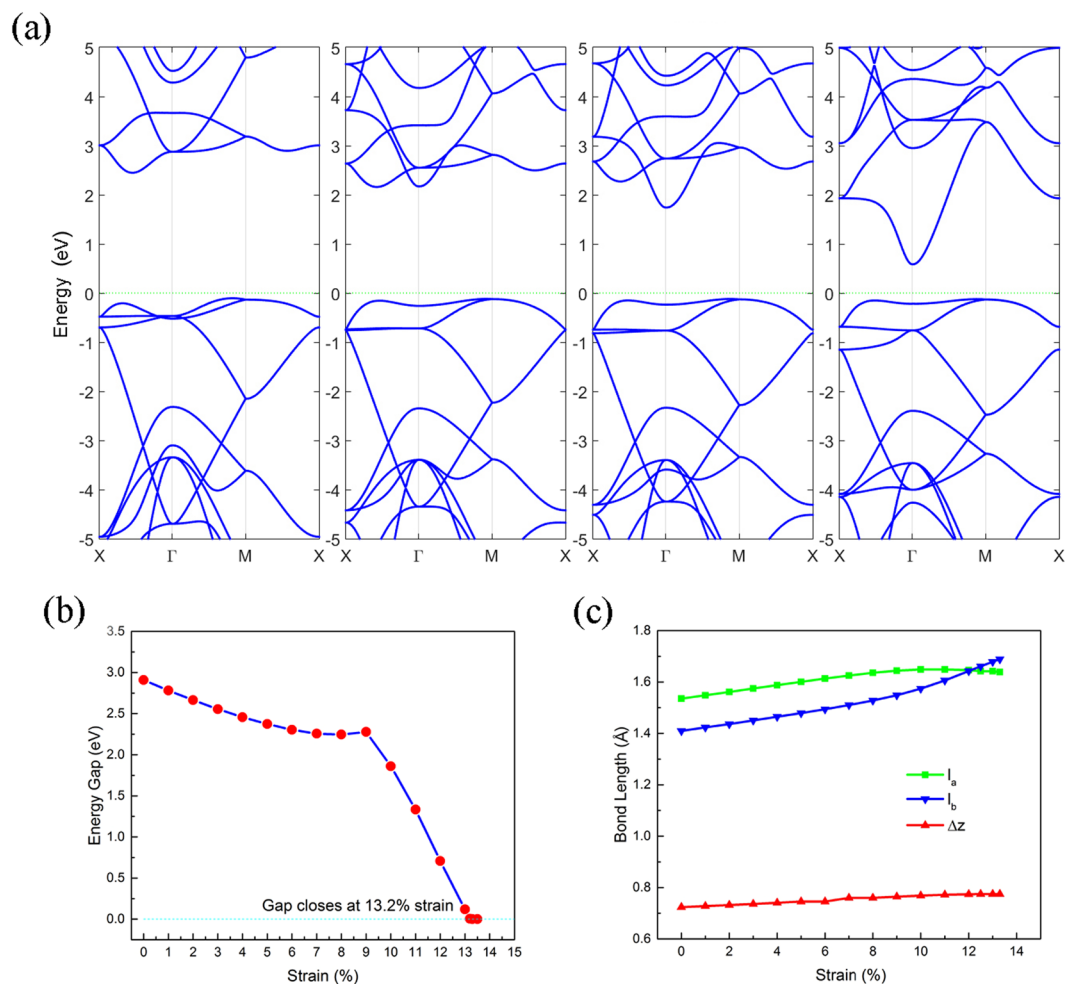
band structure using HSE functionals for comparison, as shown in Fig. 4(b). The band gap calculated using HSE functionals is 4.7 eV and the PBE result underestimates the gap by about 1.8 eV, even though these band structures near the Fermi level are similar. From the band of free ON, the conduction band minimum (CBM) is along the X- $\Gamma$  line and the valence band maximum (VBM) is along the  $\Gamma$ -M line, which means that ON is an indirect gap semi-conductor.

To further investigate the orbital feature of band structures, the projected density of states (PDOS) and projected band are calculated, as shown in Fig. 5. From Fig. 5(a–c), it is clear that the band is mainly made up of s and p orbitals, but the contributions are different. Below the Fermi level, bands in the lower energy main have more s characters, while those bands near the Fermi level have more  $p_z$  characters, which are responsible for the sharp peak near the Fermi energy in the density of states (DOS) as shown in Fig. 5(d). The lower band mainly consists of s orbitals, as shown in Fig. 5(a), while the contribution of  $p_{x+y}$  orbitals becomes greater as the energy increases as shown in Fig. 5(b).  $p_z$  orbitals play a dominant role near the Fermi level, as shown in Fig. 5(c). There is a flat band near the Fermi level, and the DOS is singular, which is mainly due to  $p_z$  orbitals.

Our previous study<sup>16</sup> has shown that the stacking of nitrogenene can change its electronic structure. The band gap decreases as the number of layers increases and some of the degeneracy of the bands is broken, especially at some high symmetry points, as shown in Fig. 6(a,b). The gap decreases rapidly as the number of layers increases. The general trend is similar for both the AA stacking and AB stacking, see Fig. 6(c,d), and the band gap is found to be linearly dependent on the reciprocal of the number of layers.

**Effect of Biaxial Tensile Strain.** In addition to multilayer stacking, tensile strain is also a frequently used technique for manipulating the band gaps of 2D materials, because it is easier to realize experimentally. Tensile strain affects the kinetic energy of electrons, which changes the band structure directly. In the process of biaxial strain, the lattice constants have been enlarged synchronously and the atoms have been relaxed again. In Fig. 7(a), the band gap decreases with the strain, decreasing slowly in the range before 8%. Interestingly, there is a small maximum at a strain of 9%, then the gap decreases more rapidly and is almost linear as the strain exceeds 9%. The gap eventually closes at the strain of 13.2%, and the system becomes a metallic state, which is a second order phase transition. The relaxation results indicated that the ON structure was still stable at the strain of 13.2%. In the process of strain, some bands shift toward to the Fermi level. However, some bands shift up and away from it.

Figure 7(b) shows the dependence of the energy gap on strain. In the beginning, the CBM is located at a point along the X- $\Gamma$  line in the Brillouin zone. The CBM then shifts to the  $\Gamma$  point when the strain reaches 9% or above.



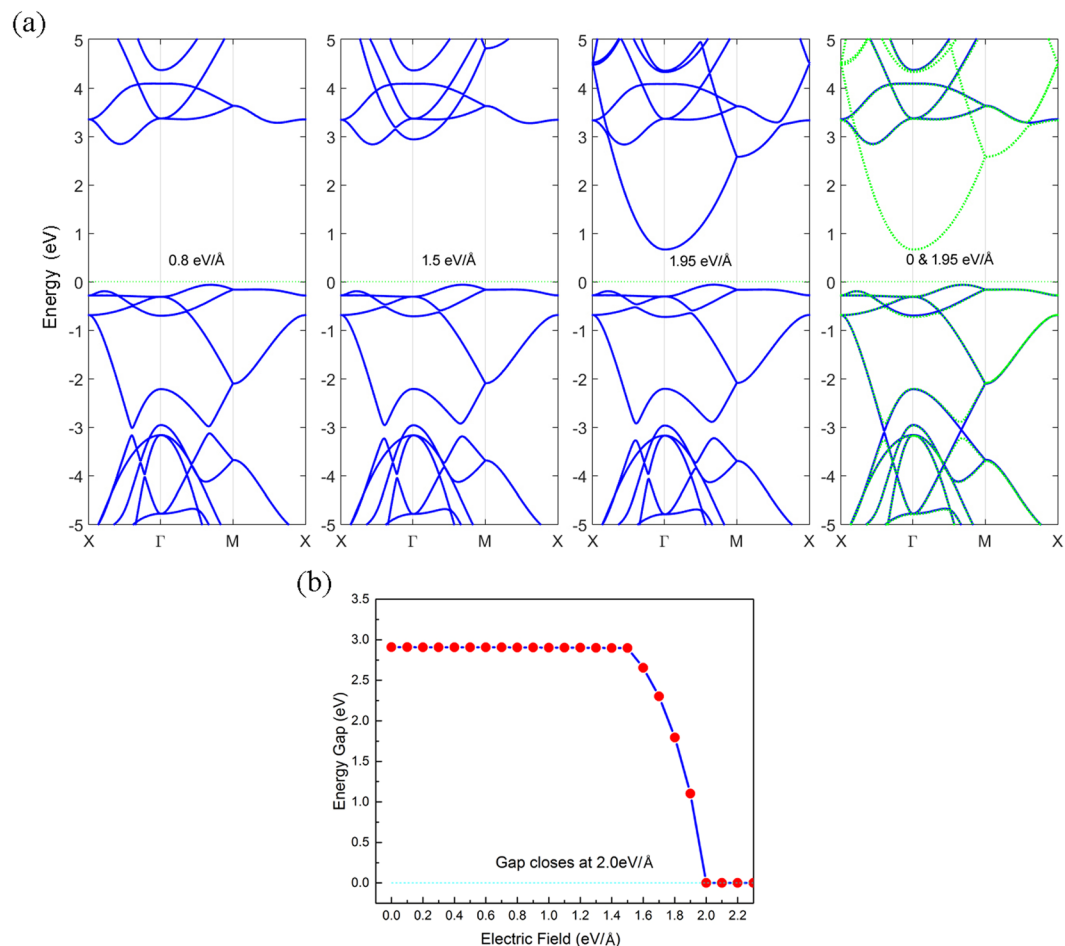
**Figure 7.** (a) Band structures of ON under the 3%, 9%, 10%, and 12% strains. (b) Dependence of energy gap on the strain. (c) Dependence of the covalent bond length  $l_a$  (green),  $l_b$  (blue) and buckling distance (red) on strain.

Figure 7(c) shows the change of structural parameters with respect to tensile strain. Without strain,  $l_a$  is longer than  $l_b$ , and both  $l_a$  and  $l_b$  are monotonically increasing with respect to strain. As strain reaches 12% or more,  $l_a$  becomes shorter than  $l_b$ .

**Effect of an External Electric Field.** The application of an external electric field is also a useful technique to control the band structure of 2D materials. From Fig. 8(a) we can see that the band structure changes as the electric field strength increases. In the beginning, the CBM stays on the X- $\Gamma$  line in the Brillouin zone but CBM shifts to  $\Gamma$  point when the electric field reaches  $1.5 \text{ eV/\AA}$  or more. However, with the increases of the field strength, some bands shift down but some bands remain unchanged. For comparison, we plot the band structure in the absence of an external electric field and in the presence of an electric field of  $1.95 \text{ V/\AA}$ , together, in the fourth panel of Fig. 8(a). The gap opens at 3 eV below Fermi level under the presence of the electric field. The band gap does not change until the field strength reaches electric field of  $1.5 \text{ eV/\AA}$  but the high energy bands move toward to the Fermi level. When the electric field reaches  $1.5 \text{ eV/\AA}$ , the band gap decreases rapidly and closes at  $2.0 \text{ eV/\AA}$ . The system then becomes metallic, as shown in Fig. 8(b). Some other materials<sup>16,24,25</sup> such as nitrogen also show similar phenomenon, due to the electron density redistributed under the electric field<sup>26,27</sup>. However, the critical field for transition is much higher than for nitrogen.

## Discussion

In this study, the stability and electronic structure of ON have been studied by first-principle calculations. Phonon dispersion, as well as first-principle molecular dynamics (MD) suggest that ON is stable. The MD result shows the ON lattice is dynamically stable at 300 K without breaking the bonds, and that wrinkles and ripples are present at finite temperatures, which indicates the structure is stable at room temperature. Results based on the density functional theory calculation suggest that ON is a semiconductor with an indirect band gap of  $2.9 \text{ eV}/4.7 \text{ eV}$  (PBE functional/HSE06 functional), which is the widest one in the octagon monolayer of group V elements. Analysis of the orbital character of the band structure is very helpful in constructing the tight-binding model, which would be beneficial for further study of its properties. In addition to monolayer ON, we also studied the electronic



**Figure 8.** (a) Band structures of ON in the presence of a perpendicular electric field. (b) Dependence of energy gap on the field strength.

structure of multilayer ON. Both the AA stacking and AB stacking can decrease the band gap and have almost the same band gap for multilayer ON. Biaxial tensile strain can decrease the band gap as well, and a nearly linear dependence of gap on strain is found when the strain is between 9% and 13.2%, where the gap closes. Moreover, the perpendicular electric field can lower the energy of bands far above the Fermi level while keeping the ordinary bands intact. We therefore found that the gap remains the same at the range of from zero to  $1.5 \text{ eV}/\text{\AA}$  but begins to decrease as the electric field strength reaches  $1.5 \text{ eV}/\text{\AA}$  and closes at  $2.0 \text{ eV}/\text{\AA}$ . Though the critical electric field is much high, this perhaps can be realized by the substrate. This study suggests that ON is a wide band gap semi-conductor and that its electronic structure can be tailored by several techniques. Our results suggest that further analysis using other methods, such as vacancy, doping and adsorption may demonstrate the existence of other interesting phenomena in the ON system, such as the existence of a Dirac cone or additional topological properties<sup>29</sup>. The transport properties of ON may exhibit some interesting phenomena, which could be seen by combining the density functional theory with the nonequilibrium Green's function formalism<sup>30</sup>. We expect that ON can be further stabilized when assembled on a substrate, because the rotational freedom will be quenched. The real ON can possibly be synthesized by comprising non-hexagonal rings with nitrogen molecules on Au(111) surfaces. This new novel material may be expected to be of use in many fields such as electronics, semiconductors, optics and spintronics.

## Methods

The material and electronic structure of ON have been calculated using the VASP code<sup>28</sup> based on PAW with PBE of exchange-correlation. The system satisfied the periodic boundary conditions with the vacuum at least  $15 \text{ \AA}$  thick between the interlayer. In order to obtain the stable structure, ions have relaxed by the conjugate-gradient method until the total force on each ion is less than  $0.01 \text{ eV}/\text{\AA}$ , then it is further relaxed by a quasi-Newton algorithm until the total force on each ion is less than  $0.0001 \text{ eV}/\text{\AA}$ . Phonon dispersions have been calculated by RESCU with a  $2 \times 2 \times 1$  supercell<sup>31</sup>. In the self-consistent calculation, an  $8 \times 8 \times 1$   $k$ -point mesh with Monkhorst-Pack scheme was used for sampling the Brillouin zone under the perpendicular electric field and a  $20 \times 20 \times 1$  grid with Monkhorst-Pack scheme was used for other conditions. The MD simulations have been performed by using an NVT ensemble for a  $4 \times 4 \times 1$  supercell at 200 K and 300 K. We have not considered the spin-orbit coupling during the calculation because it is negligibly small in the ON.

## References

- Novoselov, K. S. *et al.* Electric Field Effect in Atomically Thin Carbon Films. *Science* **22**, 666 (2004).
- Neto, A. H. C., Guinea, F., Peres, N. M. R., Novoselov, K. S. & Geim, A. K. The electronic properties of graphene. *Review of Modern Physics* **81**, 109 (2009).
- Cahangirov, S., Topsakal, M., Aktürk, E., Şahin, H. & Ciraci, S. Two- and One-Dimensional Honeycomb Structures of Silicon and Germanium. *Physical Review Letter* **102**, 236804 (2009).
- Zhu, F. F. *et al.* Epitaxial growth of two-dimensional stanene. *Nature Materials* **14**, 1020 (2015).
- Zhu, Z. & Tománek, D. Semiconducting Layered BluePhosphorus: A Computational Study. *Physical Review Letter* **112**, 176802 (2014).
- Guan, J., Zhu, Z. & Tománek, D. Phase Coexistence and Metal-Insulator Transition in Few-Layer Phosphorene: A Computational Study. *Physical Review Letter* **113**, 046804 (2014).
- Carvalho, A. *et al.* *Nature Reviews Materials* **1**, 16061 (2016).
- Liu, H. *et al.* Phosphorene: an unexplored 2D semiconductor with a high hole mobility. *ACS NANO* **8**, 4033 (2014).
- Castellanos-Gomez, A. *et al.* Isolation and characterization of few-layer black phosphorus. *2D Materials* **1**, 025001 (2014).
- Zhang, J. L. *et al.* Epitaxial Growth of Single Layer Blue Phosphorus: A New Phase of Two-Dimensional Phosphorus. *Nano Letters* **16**, 4903 (2016).
- Sheng, X. L. *et al.* Octagraphene as a versatile carbon atomic sheet for novel nanotubes, unconventional fullerenes, and hydrogen storage. *Journal of Applied Physics* **112**, 074315 (2012).
- Liu, M. *et al.* Graphene-like nanoribbons periodically embedded with four- and eight-membered rings. *Nature Communications* **8**, 14924 (2017).
- Kamal, C. & Ezawa, M. Arsenene: Two-dimensional buckled and puckered honeycomb arsenic systems. *Physical Review B* **91**, 085423 (2015).
- Oostinga, J. B., Heersche, H. B., Liu, X. L., Morpurgo, A. F. & Vandersypen, L. M. K. Gateinduced insulating state in bilayer graphene devices. *Nature Materials* **7**, 151 (2007).
- Lee, J., Tian, W. C., Wang, W. L. & Yao, D. X. Two-Dimensional Pnictogen Honeycomb Lattice: Structure, On-Site Spin-Orbit Coupling and Spin Polarization. *Scientific Reports* **5**, 11512 (2015).
- Li, J. S., Wang, W. L. & Yao, D. X. Band Gap Engineering of Two-Dimensional Nitrogen. *Scientific Reports* **6**, 34177 (2016).
- Zhang, Y., Lee, J., Wang, W. L. & Yao, D. X. Two-dimensional octagon-structure monolayer of nitrogen group elements and the related nano-structures. *Computational Materials Science* **110**, 109 (2015).
- Jeong, H. M. *et al.* Nitrogen-doped graphene for high-performance ultracapacitors and the importance of nitrogen-doped at basal planes. *Nano Letter* **11**, 2472 (2011).
- Li, X. L., Wang, X., Zhang, L., Lee, S. & Dai, H. Chemically derived, ultrasoft graphene nanoribbon semiconductors. *Science* **319**, 1229 (2008).
- Wang, X. R. *et al.* Room-Temperature All-Semiconducting Sub-10-nm Graphene Nanoribbon Field-Effect Transistors. *Physical Review Letter* **100**, 206803 (2008).
- Schedin, F., Geim, A. K. & Morozov, S. V. *et al.* Detection of individual gas molecules adsorbed on graphene. *Nature Materials* **6**, 652 (2007).
- Joshi, R. K. *et al.* Graphene films and ribbons for sensing O<sub>2</sub>, and 100 × 10<sup>-6</sup> of CO and NO<sub>2</sub> in practical conditions. *Journal of Physical Chemistry* **114**, 6610 (2010).
- Li, P. & Luo, W. A new structure of two-dimensional allotropes of group V elements. *Scientific Reports* **6**, 25423 (2016).
- Wu, Q., Shen, L., Yang, M., Cai, Y., Huang, Z., Feng, Y. P. Electronic and transport properties of phosphorene nanoribbons. *Physical Review B* **92**, 035436 (2015).
- Pramanik, A. & Kang, H. S. Giant Stark effect in double-stranded porphyrin ladder polymers. *The Journal of Chemical Physics* **134**, 094702 (2011).
- Zhao, M. *et al.* Strain-driven band inversion and topological aspects in Antimonene. *Scientific Reports* **5**, 16108 (2015).
- Kumar, P. *et al.* Thickness and electric-field-dependent polarizability and dielectric constant in phosphorene. *Physical Review B* **93**, 195428 (2016).
- Kresse, G. & Furthmüller, J. Efficient iterative schemes for *ab initio* total-energy calculations using a plane-wave basis set. *Physical Review B* **54**, 11169 (1996).
- Yu, X. L., Huang, L. & Wu, J. From a normal insulator to a topological insulator in plumbene. *Physical Review B* **95**, 125113 (2017).
- Chen, J., Hu, Y. & Guo, H. First-principles analysis of photocurrent in graphene PN junctions. *Physical Review B* **85**, 155441 (2012).
- Michaud-Rioux, V., Zhang, L. & Guo, H. RESCU: A real space electronic structure method. *Journal of Computational Physics* **307**, 593 (2016).

## Acknowledgements

The authors thank Cenke Xu, Yu Zhang, Yijie Zeng, Changwei Wu, and Matthew J. Lake for helpful discussions. W.L. and D.X.Y. are supported by the National Key R&D Program of China 2017YFA0206203, NSFC-11574404, NSFC-11275279, NSFG-2015A030313176, the Special Program for Applied Research on Super Computation of NSFC-Guangdong Joint Fund, Three Big Constructions—Supercomputing Application Cultivation Projects, and the Leading Talent Program of Guangdong Special Projects. J.L. is supported by the NSFC-11747108, Opening Project of Guangdong High Performance Computing Society (2017060103), and High-Level Talent Start-Up Research Project of Foshan University (Gg040934). S.D.L. is supported by the Natural Science Foundation of Guangdong Province (No. 2016A030313313). All calculations in this work were performed on the Tianhe-2 supercomputer with the help of engineers from the National Supercomputer Center in Guangzhou and Paratera.

## Author Contributions

W.L. and J.L. performed all the first-principle calculations and analyzed the results of these calculations. W.L.W. was in charge of commercial software usage. D.X.Y. was the leader of this study. W.L., J.L., S.D.L., and D.X.Y. wrote the paper and all authors commented on it.

## Additional Information

**Competing Interests:** The authors declare that they have no competing interests.

**Publisher's note:** Springer Nature remains neutral with regard to jurisdictional claims in published maps and institutional affiliations.



**Open Access** This article is licensed under a Creative Commons Attribution 4.0 International License, which permits use, sharing, adaptation, distribution and reproduction in any medium or format, as long as you give appropriate credit to the original author(s) and the source, provide a link to the Creative Commons license, and indicate if changes were made. The images or other third party material in this article are included in the article's Creative Commons license, unless indicated otherwise in a credit line to the material. If material is not included in the article's Creative Commons license and your intended use is not permitted by statutory regulation or exceeds the permitted use, you will need to obtain permission directly from the copyright holder. To view a copy of this license, visit <http://creativecommons.org/licenses/by/4.0/>.

© The Author(s) 2018